Air path and combustion controls coordination in diesel engine

Multi-fidelity modelling of wave energy converter farms

B. Battisti & G. Bracco
Department of Mechanical and Aerospace Engineering, Politecnico di Torino, Torino, Italy

M. Bergmann
Université de Bordeaux, IMB, UMR 5251, F-33400 Talence, France
Equipe-project Memphis, Inria Bordeaux-Sud Ouest, F-33400 Talence, France

ABSTRACT: Wave energy is considered one of the main actors in the decarbonization plan of the European Union. To drive the technologies to commercial power production, numerical simulations of wave energy converter farms are necessary. The design of such arrays is non-trivial because of the large area that multiple devices cover and the complexity of the hydrodynamics involved, that must take into account both the wave field close to the converter, and the wave propagation in the far-field. Motivated by the intrinsic necessity of high-fidelity, yet computationally efficient, dynamical models for arrays of wave energy systems, a versatile multi-fidelity model is presented, coupling the CFD method for the near-field in a small domain around the device, and a Reduced Order Model (ROM) for the far-field. The significant drop in the computational cost of the numerical simulation of wave energy converter farms permitted by this innovative coupling methodology facilitates its implementation in optimization strategies.

1 INTRODUCTION

The energy sector is responsible for more than 75% of the European Union's greenhouse gas emissions. In order to cope with the EU's ambitious objectives of cutting the greenhouse gas emissions by at least 55% by 2030 compared to 1990, a big effort must be done in the energy sector. For this reason, the Commission proposed to raise the 2030 targets to at least 40% renewable energy sources in the EU's overall energy mix (EU). In this framework, blue energy has a huge potential, as it provides a vast and predictable renewable resource. Even though wave energy is less mature with respect to other renewable energies such as solar and wind, it has the advantage of being more dense, predictable, and persistent (Sasaki 2017). Moreover, Europe is highly exposed to marine areas, offering the possibility of exploiting wave power from high to moderate resources (Lavidas & Blok 2021). Indeed, there are many WEC prototypes in Europe, at different Technology Readiness Level (TRL), both deployed in the ocean, like the point absorber by CorPower or that designed by Waves4Power, the overtopping platform by Wave Dragon, the hybrid platform WAVEGEM by GEPS Techno, the membrane-style WEC mWave by Bombora Wave Power or the OWC Mutriku (Torre-Enciso et al. 2009), and at sea, like the onshore point absorber by Eco Wave Power and the rotating mass generator ISWEC, among other technologies (see e.g. (MOREnergyLab , Mattiazzo 2019)). Nevertheless, for a technology to become competitive, it must be deployed in farms. Arranging multiple converters together is the necessary step to bring the power production from the waves to commercial scale (Ruehl & Bull 2012). Mooring systems and underwater cables may be shared among the devices, as well as the equipment production, installation, maintenance, and management. In this way, the Levelized Cost of Energy (LCOE) of a wave farm over its lifetime would be competitive.

Before the deployment of arrays in the sea, the interactions of the devices, their layout and distances, must be simulated numerically to make the best choice among maximum power production, minimum energy cost and industrial feasibility. Since wave farms can comprise a large number of devices and extend for kilometers, numerical simulations are computationally demanding. There are different approaches to numerically simulate WEC arrays, principally potential flow theory (Borgarino et al. 2012, Sarkar et al. 2014) and semi-analytical techniques based on such a principle, like the point-absorber or the plane-wave methods (Simon 1982, Mavrakos & McIver 1997), but also Boussinesq or mild-slope wave models (Venugopal et al. 2010, Beels et al. 2010) and spectral wave models (Atan et al. 2019). All these techniques have an affordable computational cost and can be used in sim-

ulations of large arrays (9, 16, 25 WECs), but they rely on several simplifying hypotheses. CFD models are more accurate but their high computational cost makes them difficult to apply for large arrays; for instance, (Devolder et al. 2017) managed to perform a CFD simulation of a 5-WECs array.

In addition to an acceptable computational cost, the choice of using a single numerical model for detecting all the different types of hydrodynamics that develop in a farm, is limiting. To overcome the obstacle of accurately describing the near-field and far-field effects present in a WEC farm, different solvers can be combined, one for the resolution of the wave-structure interaction, and another for the wave propagation. For example, (Stratigaki 2014) and (Verao Fernandez et al. 2018) propose a general methodology coupling two linear solvers, MILDwave for the wave propagation and, respectively, WAMIT and NEMOH for the wave structure interaction. (Singh & Babarit 2014) couples BEM and plane-wave approximation for the simulation of 25 heaving point absorbers and 25 surging flaps.

In this paper, a coupling strategy is proposed involving CFD and ROM models. CFD is indeed the most accurate technique for the near-field, and its high computational cost can be limited if applied to a small domain around the device, where non-linearities are dominant. Concerning the far-field, ROM allows a significant reduction in the problem dimension but preserves its characteristics, since it is based on CFD results. The resulting numerical simulation allows a precise description of the dynamics of an array, at an acceptable overall cost.

The reminder of this paper is structured as follows. In Section 2, we recall the main issues to consider when defining the numerical simulation of a WEC farm and the general coupling technique. In Section 3, the solvers chosen for this study, CFD and ROM are briefly described, and their implementation in the proposed coupling methodology is presented and applied to a case study. Finally, conclusions are drawn in Section 4.

2 NUMERICAL SIMULATIONS OF WEC FARMS

Numerical simulations of a single wave energy converter are well-known and studied within the available literature, at all levels of fidelity, from the frequency domain to the time domain, covering linear potential theory towards CFD. The hydrodynamics of a WEC are, thus, well-known, as well as the behavior of the device when coupled with the corresponding mooring system and the Power Take-Off actuator. When it comes to arrays, the simulations quickly become more complex, given the large scale represented and the different dynamics involved. Indeed, two different fields can be distinguished: a near-field, close to the device, and a far-field, which represents the wave propagation farther from the body. Arranging multiple WECs in a relatively limited area certainly generates interactions among devices, strongly affecting the wave field. Different contributions are identified, as in Figure 1, and their sum defines the perturbed wave field $\psi_P = \psi_I + \psi_R + \psi_D$.

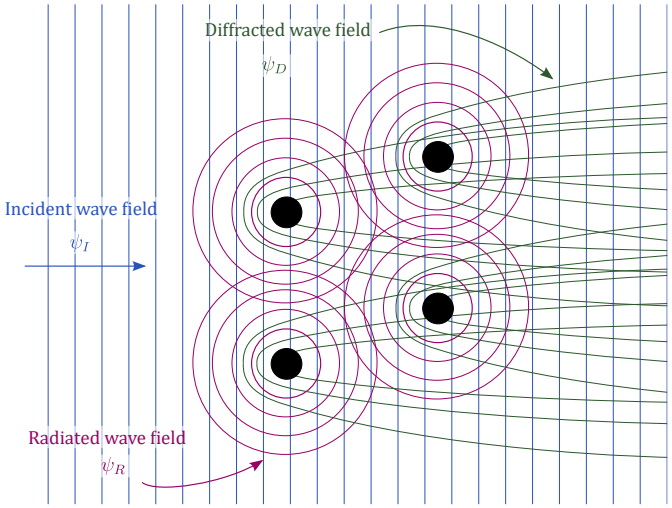

Figure 1: Visual representation of the different contributions to the perturbed wave field.

In particular, the incident wave field ψ_I represents the incoming, undisturbed, wave train; the radiated wave field ψ_R is generated from the oscillations of the converter; the diffracted wave field ψ_D is due to the change in direction of the incident field because of the presence of the device. The latter can become more complex in this array case, as, in presence of many WECs, the wave which is diffracted by a device is not only ψ_I, but is composed of the radiated and diffracted fields of all the devices around it that reach the body, and are thus also diffracted by its presence. All those contributions define the *intra*-arrays effects, and their propagation in the distance around the wave farm defines the *extra*-array effects.

The involvement of such different scales to the same numerical simulation difficults its implementation, sometimes requiring a set of simplifying assumptions. For example, the axisymmetrical feature of the point absorber, or its motion limited to the heave degree of freedom only, yield a quite simple configuration. Not surprisingly, it is thus the most implemented WEC type in arrays simulations, together with the flap type, which is characterized by only one degree of freedom as well (surge). However, the types of WECs are various and characterized by multiple degrees of freedom, which make simplifications highly unlikely. Furthermore, increasing the number of devices for larger arrays raises the computational cost of the simulation for every type of model selected, even for the potential theory case. These considerations motivate the need of a general coupling methodology that can describe the wave-structure interaction of any class of WEC, as per the CFD case,

but highly reducing the computational cost. We show that this is possible via appropriate model order reduction.

2.1 *Coupling*

To exploit the suitability of different solvers to different scales, and to dissociate from WEC type-dependence and obtain a more generalized methodology, the choice of coupling is often exploited.

Numerous numerical models have been developed for the simulation of wave energy converters, each one of them with characteristics that make it more suitable, in terms of underlying hypotheses and computational cost, for different aspects of wave farms. In particular, one can distinguish between wave-structure interaction solvers, the ones appropriate for the characterization of the device dynamics in the near-field, and wave propagation solvers, most suited for the transport of the wave trains in the far-field. For the former kind of solvers, Boundary Element Method (BEM), Smoothed-Particle Hydrodynamics (SPH) and CFD are surely the most employed. For the latter, wave propagation, models based on Boussinesq equations and mild-slope equations or spectral wave models. The complete description of all the numerical models is beyond the scope of this paper; for more information, the reader should refer to (Folley et al. 2012).

In addition to the choice of the solvers in the coupling method, the type of link between the two of them must also be chosen, either one-way or two-way. The main steps are the same in both cases: an incident wave field is given as an input for the wave-structure interaction solver of each body, which gives the radiated and diffracted wave field as output, that are then used by the wave propagation solver in addition to the incident wave field to provide the perturbed wave field and propagate it throughout the domain. The difference is that in a one-way coupling, the wave field for each body is calculated independently and then simply superposed, while in a two-way coupling there is an exchange of information between the two solvers for all the bodies, at each time-step. It is evident that a two-way coupling is more accurate, as it accounts for the real interactions among the WECs, at a higher computational cost, since the solution must be re-calculated at each time-step.

3 THE CFD-ROM METHODOLOGY

In this paper, a methodology coupling CFD and ROM is proposed. It is thus important to recall the bases of the two techniques before the discussion and analysis of the strategy for their interaction.

3.1 *Computational Fluid Dynamics*

Computational Fluid Dynamics is based on Navier-Stokes equations, a set of non-linear partial differential equations, that account for viscous effects, turbulence, and two-fluids flows.

In case of an incompressible, laminar flow, with no source terms, the mass and momentum conservation equations read as:

$$\nabla \cdot \mathbf{u} = 0, \tag{1}$$

$$\frac{\partial \mathbf{u}}{\partial t} + (\mathbf{u} \cdot \nabla)\mathbf{u} = -\frac{1}{\rho}\nabla p + \frac{1}{\rho}\nabla \cdot (\mu(\nabla \mathbf{u} + (\nabla \mathbf{u})^T)) + \mathbf{g}.$$

CFD models are time-domain models, with a time discretization done using time-steps; the spatial discretization is normally based on finite volumes or finite elements meshes. Compared to other lower fidelity solvers, CFD is particularly suitable for all the hydrodynamic non-linearities, especially those significant around the WEC device. They are suitable for the detection of a free surface, even though prone to internal dissipation; however, it is a well-known shortcoming, that can be numerically handled. The main disadvantage of CFD is the computational cost, both in terms of memory and time, that makes it unaffordable to use for simulations of WEC farms.

3.2 *Reduced Order Modelling*

Model Order Reduction was originally developed in the area of systems and control theory for the simplification of dynamical systems; it was quickly applied to various other domains of numerical analysis, among which fluid dynamics, like in (Lumley 1967). There exist several ROM approaches, such as Reduced Basis (Boyaval et al. 2010), Truncated Balanced Realization (Moore 1981), Proper Generalized Decomposition (Chinesta et al. 2011), and Proper Orthogonal Decomposition (POD) (Sirovich 1987, Bergmann et al. 2009).

In this study, POD is considered, which is based on a collection of the so-called *snapshots* (Bergmann & Cordier 2008), that represent the results of experimental measurements or, as in this case, numerical simulations. Since the snapshots are collected from the CFD results, they satisfy the Navier-Stokes equations (see Eq. 1). In the POD technique, any variable of the problem, gathered here in $\mathbf{U}$, a function of time t and space $\mathbf{x} = (x, y, z)$, can be defined as a linear superposition of the so-called basis functions Φ_i, which identify the most relevant structures of the fluid flow and temporal coefficients a_i:

$$\mathbf{U}(t, \mathbf{x}) = \sum_{i=1}^{N_S} a_i(t)\Phi_i(\mathbf{x}), \tag{2}$$

where N_S represents the total number of snapshots. The reduction of the solution space is done by a truncation of the set of basis functions to a number

$N_{POD} \ll N_S$, such that the relative information content (RIC) is greater than a certain percentage value δ:

$$RIC = \frac{\sum_{i=1}^{N_{POD}} \lambda_i}{\sum_{i=1}^{N_S} \lambda_i} > \delta, \tag{3}$$

where λ_i are the eigenvalues related to the POD basis, representing the contribution given by each mode to the reconstruction of the snapshots. Using the approximation

$$\mathbf{U}(t, \mathbf{x}) \simeq \sum_{i=1}^{N_{POD}} a_i(t)\Phi_i(\mathbf{x}), \tag{4}$$

for each of the variables involved in a two-phase flow, that are $\mathbf{U} = \{\mathbf{u} = (u, v, w), p, \rho, \mu\}$, and a Galerkin projection of Eq. 1 onto the set of basis functions $\Phi = \{\Phi_i\}_{i=1}^{N_{POD}}$, the dynamic system for the vector of time coefficients a can be defined as:

$$\dot{\mathbf{a}} = (\mathbf{a}^T \underline{\mathbf{B}}\, \mathbf{a})\mathbf{a} + \mathbf{a}^T \underline{\mathbf{C}}\, \mathbf{a}, \tag{5}$$

where $\underline{\mathbf{B}}$ and $\underline{\mathbf{C}}$ are matrices corresponding to the linear and quadratic terms of Eq. 1. The derivation of such a POD model based on Galerkin projection is nontrivial for its highly non-linear nature, linked to the two-fluid nature of the problem.

For simplicity, a Galerkin-free POD model is implemented in this study to show some first results of the coupling methodology. In this approach, there is not a Galerkin projection, so the POD modes are not used to span the system dynamics, but rather to estimate it through a projection. In this way, the computation would be less sensitive to system parameters and the particular dataset used to build the POD basis, as in the case of a traditional POD-Galerkin model (Sirisup et al. 2005).

3.3 *Coupling strategy*

For the implementation of the coupling strategy, the computational domain can be divided into different zones (see Figure 2): the complete large domain Ω, the high-fidelity region Ω_{HF}, the low-fidelity region Ω_{LF}, and the boundary conditions as link between the two regions. For a simple representation, the domain is shown as bi-dimensional, but it should be clear that it is just a section of an actual three-dimensional domain. The methodology is inspired from (Bergmann et al. 2018), where it is applied to mono-fluid cases and is adapted here for a bi-fluid case.

The methodology is divided in two steps. First, an offline phase, during which a database of high-fidelity solutions on the large domain Ω is collected, for different values of several parameters such as the wave

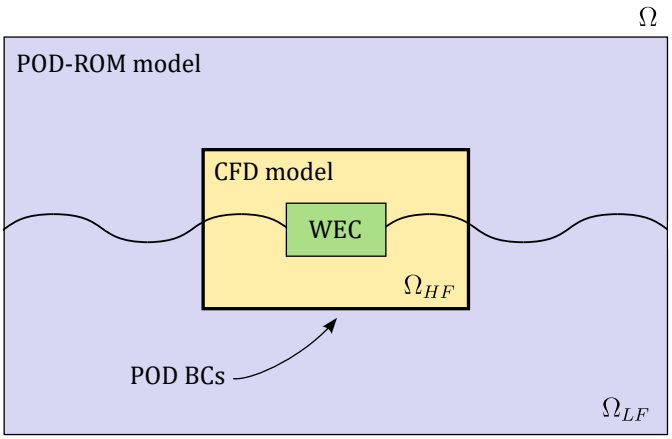

Figure 2: Bi-dimensional sketch of the computational domain decomposition.

characteristics, and considering that time is also classified as a parameter. This phase is computationally costly, but it is done only once, and is then used for an enormous amount of parameters values lying within the range of the complete dataset. During this offline phase, the set of POD spatial basis functions Φ is obtained.

In the online phase, the domain Ω is decomposed in Ω_{HF}, where the CFD model is applied, and in Ω_{LF}, where the POD-ROM model is applied. The link between the two domains are the boundary conditions of Ω_{HF}, that are imposed by the low-fidelity solution and are used to compute the high-fidelity solution. Moreover, the CFD solution is used to evaluate the temporal coefficients $\tilde{\mathbf{a}}$ that allow the reconstruction of the solution in Ω_{LF}. Such coefficients are obtained as solution of the following minimization problem:

$$\tilde{\mathbf{a}} = \arg\min_{\mathbf{a}} \left\| \mathbf{U}^{CFD} - \mathbf{U}^{POD} \right\|_2 \quad \text{on } \Omega_{HF} \tag{6}$$

where $\mathbf{U}^{CFD}$ is the high-fidelity solution and $\mathbf{U}^{POD}$ is the low-fidelity solution reconstruction at the same time-step. The algorithm can be delineated as follows:

Algorithm for coupling

At $t = t_n$
  BCs on $\Omega_{HF} \leftarrow \Omega_{LF}$
Do a timestep Δt ▷ $t = t_{n+1}$
  Compute solution in Ω_{HF}
  Solve minimization problem (eq. 6) → Compute $\tilde{\mathbf{a}}$
  Update solution in Ω_{LF}
  return updated BCs
  goto *top*.

The proposed technique is effectively a two-way coupling method, in which there is a continuous exchange of information between the two solvers, through the solution in Ω_{HF} in one direction and the boundary conditions in the opposite direction. The possibility of reducing the size of these exchange domains or blending them in a single overlapping region, as done in (Bergmann et al. 2018), is currently investigated.

Moreover, the provision of the boundary conditions obviously affects the evolution of the solution and thus must be done carefully. In this case, the temporal discretization implemented in the CFD model is implicit, so, in principle, the boundary conditions imposed by the ROM model at time t_n should be those at time t_{n+1}, which is not possible. Therefore, for a correct treatment of the coupling, multistep methods such as Adam-Bashforth type are taken into consideration, to use previous information and provide boundary conditions with a higher accuracy than the ones at t_n.

3.4 *Application to a case study*

In this section, the application of the coupling strategy to a bi-fluid case is presented. The problem analyzed is inspired from the well-known validation test of the dam break. The lateral and bottom boundaries are impermeable walls and there is free outflow at the top; the computational domain is three-dimensional, with two symmetry planes in the z-direction (see Figure 3).

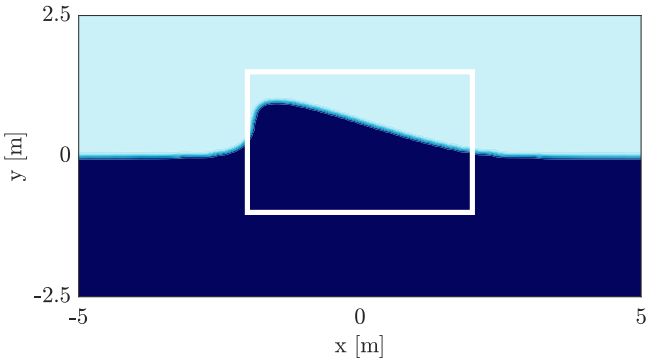

Figure 3: Bi-dimensional section of initial condition and domain decomposition for the case study.

The initial condition is a non-symmetrical free surface and is let free to evolve after $t = 0$. The fluids are not water and air but can be called *heavy* and *light* fluids, with the following properties: densities $\rho_{heavy} = 2\,\mathrm{kg\,m^{-3}}$ and $\rho_{light} = 1\,\mathrm{kg\,m^{-3}}$, and dynamic viscosities $\mu_{heavy} = 0.002$ Pa s and $\mu_{light} = 0.005$ Pa s. Referring to Figure 3, the high-fidelity domain Ω_{HF} is inside the white rectangle, representing the coupling boundary conditions, and Ω_{LF} is outside. The CFD computational domain is discretized with a Cartesian mesh, with a refinement at the free surface and the solution is interpolated on the same mesh, without refinement, for the ROM solver.

During the offline phase, a CFD simulation on Ω is conducted and $N_S = 201$ snapshots are collected at constant time-steps for 2 seconds. The variables in this case are $\mathbf{U} = \{\mathbf{u}, p, 1/\rho, \mu/\rho\}$. The Φ basis functions are computed and truncated at $N_{POD} = 21$, giving a $RIC = 99.99\%$. In this case, the dataset is limited to a single parameter variation (the time), because it is a first validation of the method; the dataset is expected to be enlarged to other parameters.

In the online phase, the computation is initialized on Ω_{HF} imposing the initial condition derived from the ROM model at $t = 0$. Then, the algorithm illustrated in Section 3.3 is implemented for ten timesteps, for two different cases: one with boundary conditions given at time t_n and the other with boundary conditions given at time t_{n+1}. The simulation is stopped and results are compared to the high-fidelity solution on Ω.

As can be seen in Figure 4, the temporal coefficients $\mathbf{a}$ obtained from the coupling are in good agreement with those obtained from the CFD results on the entire domain Ω. The comparison of the error in 2-norm (Figure 5) also shows a good behaviour of the coupling strategy in both cases. Of course, the case with boundary conditions at t_n gives higher errors, even though they still are small. The multistep method could seem superfluous in this case, but will be analyzed in order to quantify its effect and considering that there may be other case studies where the difference in the errors is larger.

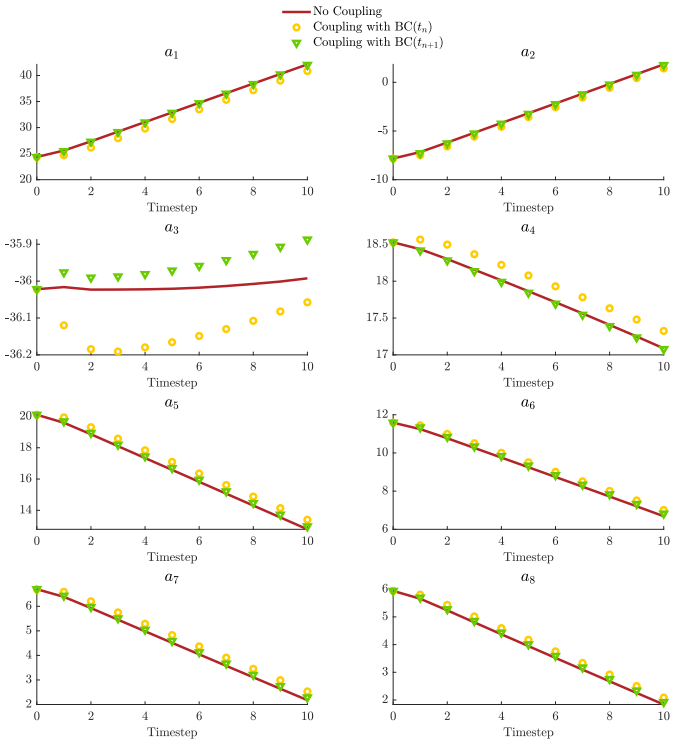

Figure 4: First 8 coefficients (of 21) computed in the two cases of POD-ROM model with respect to the projection coefficients computed from the CFD solution on Ω.

If the results of the simulations implementing the coupling strategy show a good correspondence to the CFD results, the difference in terms of mesh size is remarkable: the size of the entire domain Ω is almost five times the small domain Ω_{HF}. It corresponds to a lighter CFD simulation, both in terms of memory and computational time. At the moment, the gain in calculation time is difficult to estimate because the coupling procedure needs to be automated with a routine, but it surely is expected to reflect, at least partly, the

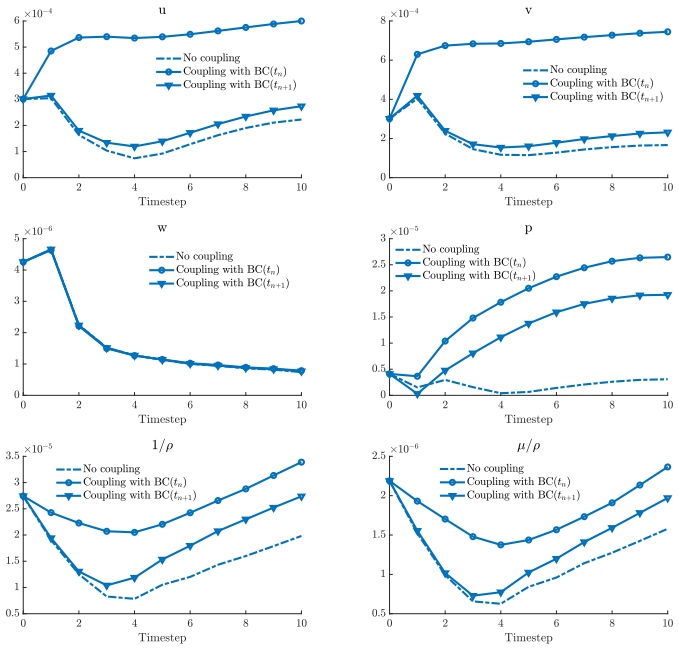

Figure 5: 2-norm errors of the POD-ROM model with respect to the CFD solution, for all the variables.

difference in mesh size. Few time-steps are, of course, not representative of the problem, but necessary to assess the correct coupling algorithm; after its automatization, a more accurate assessment of the error and of the reduction of the computational cost will be possible.

4 CONCLUSIONS

Wave energy has the potential to consistently help the European Union in its ambitious aim of becoming the first climate neutral continent by 2050. However, to produce power at a commercial scale, wave energy converters need to be deployed in farms.

Numerical simulations of such farms are the mandatory step before going to the sea, and also recommended for design or optimization studies. Due to the large dimensions of the computational domain, the simulations become quickly prohibitive in terms of memory and CPU time when the number of devices increases. A great effort is done to find numerical methods able to provide an accurate result at an affordable cost. This paper goes in this direction and proposes a coupling procedure implementing CFD models in a small domain around each device and ROM models all around. In this way, the nonlinear features of the dynamics around the devices are ensured by the high-fidelity trait of the CFD solver and the simplification done by the ROM solver is only on the dimension of the problem and not on the flow properties (like the viscosity).

Preliminary results on a test case show good representation of the dynamics of a bi-fluid flow. The procedure still needs to be automated and applied to fluids with various characteristics of density and dynamic viscosity, and also to turbulent flows. The application to a wave energy converter will then be straightforward.

REFERENCES

Atan, R., W. Finnegan, S. Nash, & J. Goggins (2019). The effect of arrays of wave energy converters on the nearshore wave climate. *Ocean Engineering 172*, 373–384.

Beels, C., P. Troch, K. De Visch, J. P. Kofoed, & G. De Backer (2010). Application of the time-dependent mild-slope equations for the simulation of wake effects in the lee of a farm of Wave Dragon wave energy converters. *Renewable Energy 35*(8), 1644–1661.

Bergmann, M., C.-H. Bruneau, & A. Iollo (2009). Enablers for robust POD models. *Journal of Computational Physics 228*(2), 516–538.

Bergmann, M. & L. Cordier (2008). Optimal control of the cylinder wake in the laminar regime by Trust-Region methods and POD Reduced-Order Models. *Journal of Computational Physics 8*, 7813–7840.

Bergmann, M., A. Ferrero, A. Iollo, E. Lombardi, A. Scardigli, & H. Telib (2018). A zonal Galerkin-free POD model for incompressible flows. *Journal of Computational Physics 352*, 301–325.

Bombora Wave Power. Bombora website. `https://bomborawave.com/mwave/` Accessed on 20/04/2022.

Borgarino, B., A. Babarit, & P. Ferrant (2012). Impact of wave interactions effects on energy absorption in large arrays of Wave Energy Converters. *Ocean Engineering 41*, 79–88.

Boyaval, S., C. Bris, T. Lelièvre, Y. Maday, N. Nguyen, & A. Patera (2010). Reduced Basis Techniques for stochastic problems. *Archives of Computational Methods in Engineering 17*, 435–454.

Chinesta, F., P. Ladeveze, & E. Cueto (2011). A short review on Model Order Reduction based on Proper Generalized Decomposition. *Archives of Computational Methods in Engineering 18*, 395–404.

CorPower. CorPower Ocean website. `https://www.corpowerocean.com` Accessed on 20/04/2022.

Devolder, B., P. Rauwoens, & P. Troch (2017). Numerical simulation of an array of heaving floating point absorber wave energy converters using OpenFOAM. *VII International Conference on Computational Methods in Marine Engineering (MARINE 2017)*.

Eco Wave Power. Eco Wave Power website. `https://www.ecowavepower.com/gibraltar/` Accessed on 20/04/2022.

EU. European Commission website. *European Commission - Energy - Topics - Renewable energy*. `https://energy.ec.europa.eu/topics/renewable-energy_en` Accessed on 20/04/2022.

Folley, M., A. Babarit, B. Child, D. Forehand, L. O'Boyle, K. Silverthorne, J. Spinneken, V. Stratigaki, & P. Troch (2012). A review of numerical modelling of wave energy converter arrays. *ASME 2012 International Conference on Ocean, Offshore and Artic Engineering (OMAE2012)*, 1–11.

GEPS Techno. GEPS Techno website. `https://www.geps-techno.com/en/autonomous-hybrid-platforms/` Accessed on 20/04/2022.

Lavidas, G. & K. Blok (2021). Shifting wave energy perceptions: The case for wave energy converter (WEC) feasibility at milder resources. *Renewable Energy 170*, 1143–1155.

Lumley, J. (1967). The structure of inhomogeneous turbulent flows. *Atmospheric Turbulence and Radio Wave Propagation (eds AM Yaglom, VI Tartarsky)*, 166–177.

Mattiazzo, G. (2019). State of the art and perspectives of wave energy in the Mediterranean sea: Backstage of ISWEC. *Frontiers in Energy Research 7*.

Mavrakos, S. & P. McIver (1997). Comparison of methods for computing hydrodynamic characteristics of arrays of wave power devices. *Applied Ocean Research 19*(5), 283–291.

Moore, B. (1981). Principal Component Analysis in linear sys-

tems: Controllability, observability, and model reduction. *Automatic Control, IEEE Transactions on 26*, 17 – 32.

MOREnergyLab. MOREnergyLab website. `http://www.morenergylab.polito.it` Accessed on 20/04/2022.

Ruehl, K. & D. Bull (2012). Wave energy development roadmap: Design to commercialization. *OCEANS 2012 MTS/IEEE: Harnessing the Power of the Ocean*, 1–10.

Sarkar, D., E. Renzi, & F. Dias (2014). Wave farm modelling of oscillating wave surge converters. *Proceedings of the Royal Society A: Mathematical, Physical and Engineering Sciences 470*(2167), 20140118.

Sasaki, W. (2017). Predictability of global offshore wind and wave power. *International Journal of Marine Energy 17*.

Simon, M. J. (1982). Multiple scattering in arrays of axisymmetric wave-energy devices. Part 1. A matrix method using a plane-wave approximation. *Journal of Fluid Mechanics 120*, 1–25.

Singh, J. & A. Babarit (2014). A fast approach coupling Boundary Element Method and plane wave approximation for wave interaction analysis in sparse arrays of wave energy converters. *Ocean Engineering 85*, 12–20.

Sirisup, S., G. Karniadakis, D. Xiu, & I. Kevrekidis (2005). Equation-free/Galerkin-free POD-assisted computation of incompressible flows. *Journal of Computational Physics 207*, 568–587.

Sirovich, L. (1987). Turbulence and the dynamics of coherent structures. i - Coherent structures. ii - Symmetries and transformations. iii - Dynamics and scaling. *Quarterly of Applied Mathematics - QUART APPL MATH 45*.

Stratigaki, V. (2014). *Experimental study and numerical modelling of intra-array interactions and extra-array effects of wave energy converter arrays*. Ph. D. thesis, Ghent University.

Torre-Enciso, Y., I. Ortubia, L. Aguileta, & J. Marqués (2009). Mutriku wave power plant: From the thinking out to the reality. *Proceedings of the 8th European Wave and Tidal Energy Conference*, 319–329.

Venugopal, V., I. Bryden, & A. Wallace (2010). On the interaction of waves with an array of open chambered structures: Application to wave energy converters. *Proceedings of the International Conference on Offshore Mechanics and Arctic Engineering - OMAE 3*.

Verao Fernandez, G., P. Balitsky, V. Stratigaki, & P. Troch (2018). Coupling methodology for studying the far field effects of wave energy converter arrays over a varying bathymetry. *Energies 11*(11).

Wave Dragon. Wave Dragon website. `http://www.wavedragon.net` Accessed on 20/04/2022.

Waves4Power. Waves4Power website. `https://www.waves4power.com` Accessed on 20/04/2022.